LANGMUIR

pubs.acs.org/Langmuir Article

Role of the Protein Corona in the Colloidal Behavior of Microplastics

Marion Schvartz,* Florent Saudrais, Stéphanie Devineau, Stéphane Chédin, Frédéric Jamme, Jocelyne Leroy, Karol Rakotozandriny, Olivier Taché, Guillaume Brotons, Serge Pin, Yves Boulard, and Jean-Philippe Renault*

Cite This: https://doi.org/10.1021/acs.langmuir.2c03237 Read Online

ACCESS | Metrics & More | Article Recommendations | Supporting Information

ABSTRACT: Microparticles of polyethylene and polypropylene are largely found in aquatic environments because they are the most produced and persistent plastic materials. Once in biological media, they are covered by a layer of molecules, the so-called corona, mostly composed of proteins. A yeast protein extract from *Saccharomyces cerevisiae* was used as a protein system to observe interactions in complex biological media. Proteins, acting as surfactants and providing hydrophilic surfaces, allow the dispersion of highly hydrophobic particles in water and stabilize them. After 24 h, the microplastic quantity was up to 1×10^{11} particles per liter, whereas without protein, no particles remained in solution. Label-free imaging of the protein corona by synchrotron radiation deep UV fluorescence microscopy (SR-DUV) was performed. *In situ* images of the protein corona were obtained, and the adsorbed protein quantity, the coverage rate, and the corona heterogeneity were determined. The stability kinetics of the microplastic suspensions were measured by light transmission using a Turbiscan analyzer. Together, the microscopic and kinetics results demonstrate that the protein corona can very efficiently stabilize microplastics in solution provided that the protein corona quality is sufficient. Microplastic stability depends on different parameters such as the particle's intrinsic properties (size, density, hydrophobicity) and the protein corona formation that changes the particle wettability, electrostatic charge, and steric hindrance. By controlling these parameters with proteins, it becomes possible to keep microplastics in and out of solution, paving the way for applications in the field of microplastic pollution control and remediation.

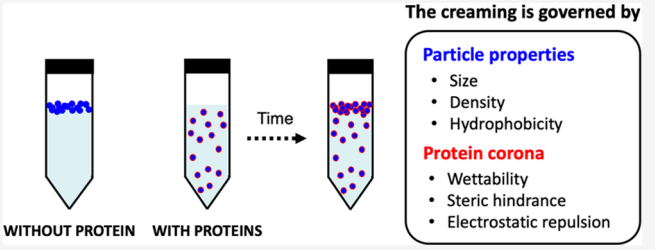

INTRODUCTION

Environmental issues related to plastic pollution have gained increasing attention in recent years, which led to an accumulation of a large amount of data concerning the extent and the nature of this pollution. When plastics are discharged in an aqueous environment, they are degraded because of UV light, mechanical stress, or by microorganisms, leading to the fragmentation of the materials.[1−5] The resulting plastic particles have a higher available surface, increasing the possibility to interact with biomolecules. Recently, the number of small microplastics (MPs, <20 μm) and nanoplastics (NPs, <100 nm to <1 μm depending on the community) has raised major concerns.[6−8] The presence of microplastics has been reported in all ecosystems. In a very recent study, the authors estimated that there are ∼25 trillion pieces of MPs in the world's upper oceans.[9]

The final fate of these microplastics depends on their degradability and colloidal behavior in the environment, namely, their tendency to cream, sediment, and aggregate. Three aspects should be considered to understand the colloidal stability of microplastics. The first one corresponds to MP intrinsic properties: it was shown that the size, density, and surface charge strongly impact the vertical behavior of MPs in a water column.[10,11] Aging may modify these intrinsic properties through surface oxidation, chain breakage, or monomer release.

The second parameter is the electrostatic stabilization that is directly driven by the medium composition. When particles are in a salted solution, an electrical double layer is formed by counterions, creating an energy barrier (DLVO theory[12,13]) that promotes particle stabilization. This electrostatic stabilization is more or less important according to the charge density. In a dispersion medium, the nature and quantity of charged compounds as well as pH modify the particle/particle interactions, impacting their colloidal stability.[14,15] Above the critical coagulation concentration (CCC), the electrostatic repulsions are not sufficient,[16] leading to aggregation and eventually creaming or sedimentation depending on the MP density.

The last key parameter in the MP fate is the nature and the quantity of the adsorbed molecules on the MP surface, sometimes described as ecorona or biocorona and composed

Received: November 29, 2022
Revised: March 7, 2023

of inorganic salts and humic acids, proteins, lipids, and nucleic acids.[17]

In addition to a density increase and surface charge modulation, it was observed that these corona could change the wettability of hydrophobic MPs, leading to a transition to a more hydrophilic surface favoring MP sinking.[18,19] The absorption of small molecules, such as hydrophobic pollutants, within the polymer matrix is also possible. However, it is expected that the solid−liquid interface formed by the adsorbed molecules and the electrical double layer will play a major role in the colloidal stability of the particles.

There is an urgent need to understand the colloidal behavior of microplastics. In this domain, knowledge has been gained from the field of nanotoxicology.[20] Indeed, micro- and nano-objects do not remain naked in the environment or in organisms but become rapidly covered by a layer of biomolecules, the so-called corona. Proteins, which are a major component of this corona,[21] give a novel biological identity to these particles, changing their toxicity,[22,23] their environmental fate[24−27] and, of interest here, their colloidal and aggregation properties. This aspect has been extensively studied in inorganic nanoparticles.[28−30]

Studies on synthetic polystyrene nanoparticles ("latex"), which have often been used as model particles for micro- and nanoplastics, suggest that the protein corona can also alter the colloidal behavior of MPs.[11,31,32] However, little data are available on the microscopic characterization of the protein corona that forms in complex biological environments and its effects on the colloidal stability of hydrophobic microplastics.

In this work, we tried to understand (i) to what extent proteins can stabilize microplastics in solution and (ii) if this stabilization depends on the properties of the protein corona.

We analyzed the protein corona's characteristics *in situ* using label-free protein imaging, and we investigated how it affects the colloidal stability of initially naked microplastics. Polyethylene (PE) and polypropylene (PP) microplastics, with a diameter <20 μm, were chosen because PE and PP are the most produced and the most long-lived components of actual plastic pollution. Furthermore, the particles have a hydrophobic surface, which is more relevant with respect to real plastic waste than the polystyrene particles currently used in most studies.[31,33,34] The chosen protein system is a Yeast Protein Extract (YPE) from *Saccharomyces cerevisiae* containing about 6000 different proteins.[35] The yeast protein extract was more specifically used because it remains the better-known complex protein mixture (structures of thousands of biomolecules described, isoelectric points, abundance). All important protein families are present (ribosomes, cytoskeleton, metabolism) and the most abundant ones in the yeast extract are indeed the most probable to be found in the realm of life and afterward in the environment.[36]

Bovine serum albumin (BSA), which is a very well-known protein whose structure and adsorption properties are largely described in the literature, was also used here as a model protein for comparison purposes.[37]

MATERIALS AND METHODS

Microplastics' Characterization. The microplastics used are a gift from Clariant (Germany), under the reference Ceridust 3610 (PE) and Ceridust 6050M (PP). They were characterized using the following techniques: optical microscopy, small-angle X-ray scattering (SAXS), X-ray photoelectron spectroscopy (XPS), Fourier transform infrared spectroscopy (FTIR), and Raman confocal microscopy.

Size distributions were determined using the Feret diameter measured using a modified inverted microscope (Zeiss Observer Z1, Germany) and analyzed using Fiji.[38]

The specific surface area was measured by SAXS. The data correspond to an average of three measurements on dry powders under vacuum carried out on a Xeuss 2.0 copper setup from Xenocs (France) with 3,600 s counting times and a sample-to-detector distance of 2.5 m.

The microplastics were also imaged by confocal Raman microscopy using a WITec alpha300 RA instrument (Oxford Instruments, Germany). Microplastics were deposited on a CaF_2 substrate (ESCO Optics). Raman images of 30 μm × 30 μm areas were acquired using a 532 nm excitation wavelength, 100× objective (NA 0.9), 600 g/mm grating, 10 mW laser power, 0.1 s exposure time, and 0.3 μm step. The corresponding bright-field image was taken in reflection mode with the same objective. The absence of laser damage was controlled by accumulating single spectra on the same spot for 50 s at the same power. Data were treated using WITec Project Five software. Cosmic rays were removed automatically and manually. The background was subtracted using shape functions. Raman images were obtained by automatically generating spectral components using the True Component Analysis feature, and the average Raman spectrum of each component was extracted. Bright-field and Raman images were exported to Fiji software.

FTIR spectra were obtained using a Bruker Tensor 27 IR (Germany) with a Specac's Golden Gate ATR accessory allowing pressing of the powder with a diamond cone; 128 scans were acquired from 500 to 5000 cm^{-1} with a resolution of 1 cm^{-1} and a scanning rate of 10 kHz.

XPS measurements were acquired using a Kratos Axis Ultra DLD spectrometer (U.K.) with monochromatic Al Kα excitation (1486.7eV) and a charge compensation system. Survey spectra were acquired at an analyzer pass energy of 160 eV and high-resolution spectra at a pass energy of 40 eV. The binding energy scale was calibrated to the C 1s line at 284.8 eV. The data were processed with CasaXPS software to calculate the percentages of atomic concentrations. The peak fitting was performed after subtracting a Shirley background. Peak areas were corrected by taking into account the Scofield sensitivity factors.

DRX measurements were performed at 40 kV and 30 mV (linear detector mode PIXel integration in continuous motion) on the "X-ray Diffraction and Diffusion" platform of IMMM following the classical measurement protocols for the powder geometry "Bragg−Brentano".

Protein Preparation. Yeast protein extracts were prepared from the *S. cerevisiae* strain BY4742 (Euroscarf), with adaptations of the protocol previously described.[39,40] Cells were grown with shaking at 30 °C in the YPD complete medium (10 g L^{-1} bacto yeast extract, 20 g L^{-1} bacto peptone, and 20 g L^{-1} glucose). Cells were collected by centrifugation, resuspended in phosphate-buffered saline (PBS) containing 5% of glycerol and a cocktail of protease inhibitors (1× EDTA-free from Thermo Fisher Scientific and 1 mM PMSF), and broken using a French press. The extract was centrifuged (4000 rpm, 15 min, 4 °C and 14,000 rpm, 40 min, 4 °C), and the supernatant containing hydrosoluble proteins were recovered.

Bovine serum albumin (BSA) was prepared using lyophilized proteins from Sigma (reference A7030). It was gently dissolved in water under stirring until a concentration of 30 g L^{-1} was reached, and then the solution was dialyzed using a 3.5 kDa cutoff (Spectra/Por) and centrifuged (15,000*g*, 5 min). Before each use, the BSA solution was centrifuged at 15,000*g* for 5 min and its concentration was checked using UV−vis spectrometry.

Adsorption Isotherms. Initially, the microplastics remained at the surface of aqueous solutions but, when proteins were introduced, their dispersion was observed, indicating that proteins are adsorbed. Equilibrium adsorption isotherms were performed by the depletion method: the amount of adsorbed proteins was calculated by subtracting the nonadsorbed protein from the total protein content. A fixed concentration of microplastics (10 g L^{-1}) was mixed with varying concentrations of proteins ranging from 0.01 to 0.7 g L^{-1} for YPE and 0.005 to 0.1 g L^{-1} for BSA in phosphate buffer (a mixture of

https://doi.org/10.1021/acs.langmuir.2c03237
Langmuir XXXX, XXX, XXX−XXX

Scheme 1. Representation of the Dispersion State without or with Proteins and the Evolution in Time of a Dispersed System

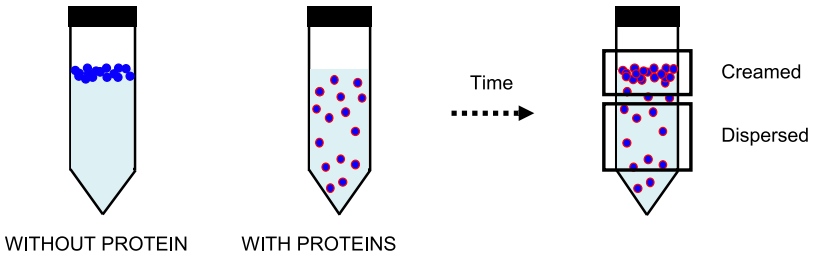

Na_2HPO_4 and NaH_2PO_4, references 28,029.292 and 28.015.294 from VWR Chemicals) at 100 mM and pH 7.0.

The exposure time was chosen to allow the visible dispersion of MPs in solution (4 h for YPE and 72 h for BSA). This time indeed corresponded to the stabilization of the protein concentration in solution after its decrease by adsorption. After gentle mixing at 4 °C, the samples were centrifuged to remove the MPs by creaming. For YPE, the protein content of the supernatants was measured using the Bradford method[41] (Sigma, reference B6916). For BSA, the concentrations were obtained by fluorescence spectroscopy (excitation: 279 nm, emission: 300−500 nm, slit width 4 nm, volume of the cuvette 200 μL). A calibration curve was measured to determine the BSA concentration from the intensity of the emission.

To compare our measurements with data found in the literature, the isotherms were fitted using a Langmuir model (eq 1).

$$m_{ads} = \frac{m_\infty \cdot K_{ads} \cdot C}{1 + K_{ads} \cdot C} \quad (1)$$

where m_∞ (mg m^{-2}) is the amount of adsorbed protein (expressed in mass per surface area to take into account the specific surface differences between MPs) and C (g L^{-1}) is the concentration of nonadsorbed proteins. The deduced constants are m_∞ (mg m^{-2}), the maximum amount of adsorbed proteins and K_{ads} (L g^{-1}), the adsorption constant (proportional to the MP/protein affinity). The saturated layers were prepared at 0.5 g L^{-1} for YPE and 0.1 g L^{-1} for BSA, whereas the unsaturated one was prepared at 0.07 g L^{-1} for YPE

Surface Tension. The surface tensions were measured with 20 μL of pendant drops after 180 s equilibrium using the Young−Laplace model. The results correspond to the average and standard deviations of three replicates.

Creaming Kinetics. Dispersions of solid particles are metastable, so they evolve to reach a state with the lowest free energy.[42] This results in a solution phase separation with creaming or sedimentation according to the particle density.

A Turbiscan LAB stability analyzer (Formulaction, France) was used to measure the destabilization kinetics of MPs in water. It corresponds here to a creaming phenomenon because of the low density of PE and PP (Scheme 1). A laser beam vertically scans the sample, and a detector measures the transmitted (detector at 0° from the incident laser) and the backscattered (detector at 135°) intensity at regular time intervals. It provides a qualitative observation of the kinetics of MP destabilization phenomena.

The light transmission values were averaged from a 5 to 18 mm sample height to extract the creaming kinetics. The mixtures of 10 mL were homogenized for 4 h at 3 rpm and 4 °C and analyzed during 24 h.

MPs Counting. Kova slides (Kova International) were used for particle quantification to determine the concentration of dispersed MPs; 10 μL of solution (MPs with proteins) was introduced, and images of five squares containing 0.1 μL each were taken with a Dino-Lite digital microscope (AM7515MT8A, Taïwan) with an ×800 magnification. Fiji software was used for image analysis.

SR-DUV Imaging. We used SR-DUV imaging to systematically analyze the properties of the protein corona *in situ* by its intrinsic fluorescence, without labeling. The images were obtained on the DISCO beamline (Zeiss Observer Z1 inverted microscope, Germany, with a replacement of the intermediate lenses that were not transparent in UV,[43,44] Synchrotron SOLEIL). The MPs were imaged in visible light because of their low intrinsic fluorescence with UV excitation (Figure S10), whereas the proteins were imaged using tryptophan and tyrosine fluorescence (excitation wavelength: 265 nm, emission wavelength: [329-351 nm]). The theoretical maximal spatial resolution can be calculated using the Rayleigh criterion (eq 2).

$$r = \frac{0.51\lambda}{NA} \quad (2)$$

where r is the Rayleigh criterion or spatial resolution, λ is the excitation wavelength, and NA is the numerical aperture. The objective was a 100× Zeiss Ultrafluar with a numerical aperture of 1.25; therefore, the theoretical maximal resolution is r = 108 nm. The fast bleaching of protein fluorescence demonstrates that the overlapping contributions can be neglected. A correction was applied to remove the beam heterogeneity (eq 3 and Supporting Information).

$$\text{corrected image} = \frac{\text{raw image} - \text{background}}{\text{illumination} - \text{background of illumination}} \quad (3)$$

The illumination corresponds to an image obtained without the sample and filter.

For YPE, two protein concentrations were chosen (0.07 and 0.5 g L^{-1}) to represent, according to the adsorption isotherms, the MP behavior before protein surface saturation and the MP behavior when proteins form a saturated layer. For BSA, only a saturation condition has been studied (0.1 g L^{-1}). In all cases, the MP concentration was 10 g L^{-1}. The samples were analyzed *in situ* without washing. A dilution step (dilution factor: 4) was realized for the samples containing 0.5 g L^{-1} proteins only to reduce the fluorescence background.

Different positions in the decantation column were compared. Because of a stability difference according to the type of MP, we collected the infranatant after 24 h of creaming for PE and after 3 h for PP MPs, which have lower colloidal stability.

Student *t*-tests were used to test the significance of the results. For a *p*-value < 0.05, the difference was considered significant.

Zetametry. ζ potentials were measured on dispersed particles from creamed samples (at rest during 24 h) on a Malvern Zetasizer using DTS1060 cells and the Smoluchowski method. PP and PE suspensions were prepared as described in DUV microscopy and diluted in phosphate buffer (100 mM, pH 7, dilution factor: 10).

Creaming Acceleration. PE particles were introduced in solution using 0.5 g L^{-1} YPE in phosphate buffer at 100 mM, pH 7 and mixed during 4 h at 3 rpm and 6 °C. To accelerate the destabilization of stable dispersions, the infranatant was collected after waiting for 60 s. Then, we compared the two treatments known to destabilize proteins: salt[45] and temperature.[46] Ammonium sulfate (Prolabo, reference 21.332.362) was introduced in the two concentrations until saturation (14% and 70% w/v), and the samples were homogenized at 3 rpm, 4 °C for 10 min. For the thermal treatment, the sample was heated at 80 °C for 1 h. After 24 h of creaming using one of the two protocols, the dispersed MPs were collected and their concentrations were determined. The results were compared with a reference sample, without a destabilization procedure.

https://doi.org/10.1021/acs.langmuir.2c03237
Langmuir XXXX, XXX, XXX−XXX

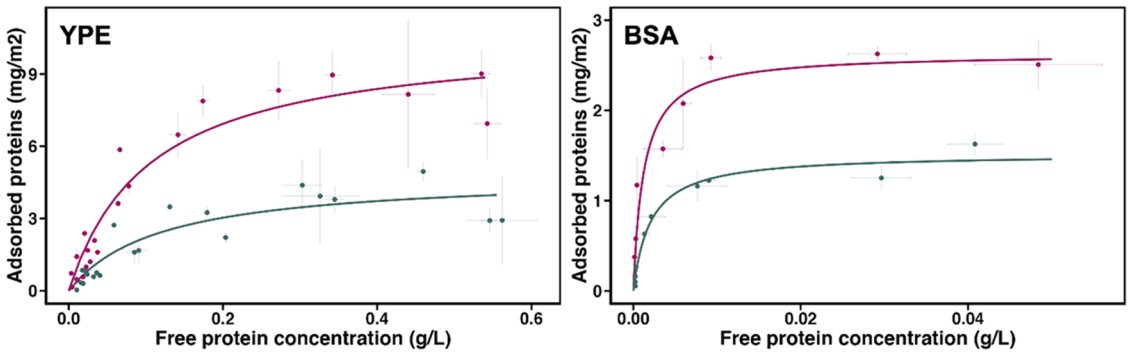

Figure 1. Adsorption isotherms of YPE and BSA on PP (purple) and PE (green) microplastics. Experimental dots and error bars correspond to the average and standard deviation of three biological replicates. The fits were obtained using a Langmuir model.

RESULTS AND DISCUSSION

Characterization of Microplastics. In addition to optical microscopy (Supporting Information Figure S1, S2, Table S1), microplastics were characterized using several methods. FTIR spectra provide information on the composition, X-ray photoelectron spectroscopy (XPS) on the surface chemistry, and Raman microscopy and small-angle X-ray scattering (SAXS) on the polymer internal structure at different scales, respectively, micrometer and nanometer. The specific surface area of the MPs was determined by SAXS.

We must notice that, if the particles present the irregular rounded shape (Supporting Information Figure S1) found for a significant proportion of environmental microplastics, they are not completely representative of microfibers which is also an abundant plastic micropollution.[47]

No additives were detected in any of the MPs by FTIR (Supporting Information Figure S3). Both MPs showed the characteristic spectra known for semicrystalline PE[48] and PP.[49] DRX analysis (Supporting Information Figures S4 and S5) showed that both orthorhombic and monoclinic phases were present in PE MPs, with little amorphous material (<10%), which can explain the relatively high density of particles (0.97). PP MPs presented the signal characteristics from isotactic polypropylene, while no amorphous phase could be detected.

Only carbon was found on the PP surface by XPS (Supporting Information Figures S6 and S7), whereas for PE, in addition to carbon, oxygen was detected, representing 0.9% of the signal. This signals a limited oxidation of the surface of PE microplastics.

The analysis of PE and PP MPs by confocal Raman microscopy showed a homogeneous structure and composition for PP particles, while local spectral differences were observed for PE particles at the micrometer scale (Figure S8). Three spectral components sharing the same vibrational bands but different intensity ratios were identified by analyzing the hyperspectral images of PE MPs (Figure S8A), while only one component was identified for PP MPs using the same method (Figure S8B). All peaks in the PP components correspond to what is expected for this polymer.[50] To compare the different PE components, we normalized the Raman spectra to the vibrational bands at 1294 cm^{-1} and 2882 cm^{-1} corresponding to the CH_2 twisting and CH_2 asymmetric stretching of PE, respectively. Differences in the intensity were observed for bands at 1062 and 1129 cm^{-1} assigned to $\nu_{as}(C-C)$ and $\nu_s(C-C)$, respectively, and at 1416, 1440, and 1464 cm^{-1} assigned to $\delta(CH_2)$ with a contribution of $\omega(CH_2)$. It was shown that the intensity of these vibrational modes is closely related to the structure and crystallinity of PE.[51,52]

In our analysis, the PE 1 component is characterized by a lower intensity of CH_2 vibrational modes at 1418 cm^{-1} previously assigned to an orthorhombic structure, and a higher intensity of the CH_2 bending mode at 1440 and 1464 cm^{-1} associated with the amorphous structure, whereas the opposite trend is observed for the PE 3 spectrum. The lower intensity of the C−C asymmetric and symmetric stretching of PE 1 compared to PE 3 is interpreted as an increase of trans chains.[51] We concluded that PE 3 corresponds to the orthorhombic phase and PE 1 to the minor amorphous phase, while PE 2, which is intermediate between these two, is tentatively assigned to the monoclinic component. Interestingly, the mapping of PE 1, PE 2, and PE 3 components delineates subdomains inside PE microplastics but not between particles, suggesting that a heterogeneous polymeric structure prevails in PE microplastics.

Small-angle X-ray scattering (SAXS) measurements are represented in Supporting Figure S9 along with the curve representing $I{\cdot}q^4$ vs q, where I corresponds to the absolute scale scattering intensity (in cm^{-1} units) and q to the scattering wave vector (in $Å^{-1}$). A clear plateau appears for q values lower than 2.5×10^{-2} $Å^{-1}$ and corresponds to a q^{-4} dependence of the SAXS apparent intensity that arises from the scattering of the interface between the polymer particles and air. From the plateau intensity level (noted $\lim(I{\cdot}q^4)$), we calculated the specific surface area expressed in m^2 g^{-1} (Table S2), using an interface scattering length density contrast $\Delta\rho b$ (9.4 and 8.72 for PE and PP, respectively, in 10^{10} cm^{-2} units) and the mass density ρ_m (0.97 for PE and 0.9 for PP in g cm^{-3}), from eq 4.[53]

$$\sigma_m = \frac{\lim_{q\to 0}(I{\cdot}q^4)}{2\pi\rho_m(\Delta\rho b)^2} \quad (4)$$

The values obtained in this way (Table S2) are measured independently of the powder compactness. The comparison of these values with the calculated surface areas for perfect spheres using the measured radii (respectively, 1.5 and 0.7 m^2 g^{-1} for PE and PP) shows that the particle surface is rather smooth with low roughness.

For the PP powder, a correlation peak was also observed at $q = 8 \times 10^{-2}$ $Å^{-1}$. It reveals, following the Hosmann model, a system of stacked lamellae of crystallized polymer chains that are constituents of larger-scale spherulites, separated by amorphous domains.[54] This lamellar organization is expected for such plastic materials and has already been docu-

https://doi.org/10.1021/acs.langmuir.2c03237
Langmuir XXXX, XXX, XXX−XXX

mented.[55,56] Such a spatial organization is too small to be observed by confocal Raman microscopy.

Proteins Adsorb on Microplastics. MPs have a low density and strong hydrophobicity. Therefore, the particles stay on the surface of aqueous solutions and avoid contact with water, even under vigorous stirring. When proteins are added to the solution, MPs are dispersed in the bulk solution (Scheme 1 and Supporting Figure S11) since proteins adsorb on the MP surface and act as surfactant systems. To quantify protein adsorption, we measured the adsorption isotherms of YPE (Figure 1, left) and BSA (Figure 1, right) on PP and PE MPs in phosphate buffer 100 mM at pH 7.

The adsorption isotherms were fitted using a Langmuir model, a widely used two-parameter isotherm model, which assumes that adsorption is reversible and limited to one molecular layer, to compare our data with values reported in the literature for a large range of proteins and solid substrates. Here, m_∞ corresponds to the maximum amount of adsorbed protein (per unit area) in mg m^{-2} and K_{ads} to the adsorption constant in L g^{-1}, proportional to the affinity.

For both protein systems, the results indicate that a saturated protein layer, the corona, is formed at high protein concentrations on PE and PP MPs. The m_∞ values correspond to nanometric layers of protein (see Table S5), much thinner than known ecoronas.[17]

The more salient observation is that, from the values of m_∞, the corona appears significantly thicker on PP than on PE MPs (Table 1). Even if data on protein adsorption on PP are scarce in the literature, this tendency was also observed for purified proteins, with a serum albumin coverage of about 1.8 times higher on PP films compared to polystyrene films.[57] The surface chemistry is slightly different between PE and PP MPs (Figure S7) with only carbons on the PP surface, whereas there are oxidation sites on the PE surface. This could explain in part the difference in the quantity of adsorbed proteins.

Table 1. Maximum Adsorption (m_∞) and Adsorption Constants (K_{ads}) of YPE and BSA on PE and PP Microplastics Determined from Adsorption Isotherms using a Langmuir Model

		m_∞ (mg m^{-2})	K_{ads} (L g^{-1})
YPE	PE	4.8 ± 0.9	8.5 ± 2.7
	PP	10.6 ± 1.1	9.5 ± 4.2
BSA	PE	1.5 ± 0.1	5.10^2 ± 1.10^2
	PP	2.6 ± 0.2	8.10^2 ± 3.10^2

m_∞ is higher for YPE than for BSA (Table 1), which can be explained by the contribution of large protein complexes in the extract (e.g., ribosomes, transcription factors, chaperones). The adsorption constants K_{ads} are significantly higher for BSA than for YPE on both MPs, indicating a stronger global affinity of purified BSA in comparison with the average affinity of the total set of proteins in YPE, which produces a more diverse corona.

For YPE, the m_∞ coverage values are comparable to the ones measured on silica nanoparticles exposed to a similar protein extract.[58] K_{ads} are slightly higher for MPs compared to silica, but we must keep in mind that the comparison of K_{ads} is more complex as this adsorption constant depends on the size and the local curvature of the particles and not only on material surface properties.[59,60]

For BSA, K_{ads} and m_∞ are in the same range as those obtained with other purified proteins such as transferrin, macroglobulin, and hemoglobin on raw and flat polymer surfaces.[61,62]

In the following experiments, we selected two exposure conditions to analyze the stabilization of MPs in solution by proteins: (i) a protein concentration lower than the isotherm plateau, corresponding to an unsaturated protein layer on MPs (UL) and (ii) a protein concentration equal to the isotherm plateau, corresponding to a saturated layer on MPs (SL).

Proteins Stabilize Microplastic Dispersions. As previously explained, the adsorption of proteins allows MPs to enter aqueous media. The wettability of MPs in the presence of proteins can be connected to their action as surfactants (Table S3). The stability of MP dispersions was characterized by the measurement of creaming kinetics using a Turbiscan analyzer, to compare the surfactant power of proteins according to the protein nature, corona saturation, and MP composition.

The transmission profiles shown in Figure 2 provide information on the dispersion state of PE and PP MPs with and without proteins as a function of time. The minimal transmission corresponds to an opaque sample with a lot of dispersed particles, whereas a translucent one exhibits maximal light transmission and corresponds to a low amount of dispersed MPs. From the transmission profiles in Figure 2, we observed the presence of a lag phase, a creaming phase, and an

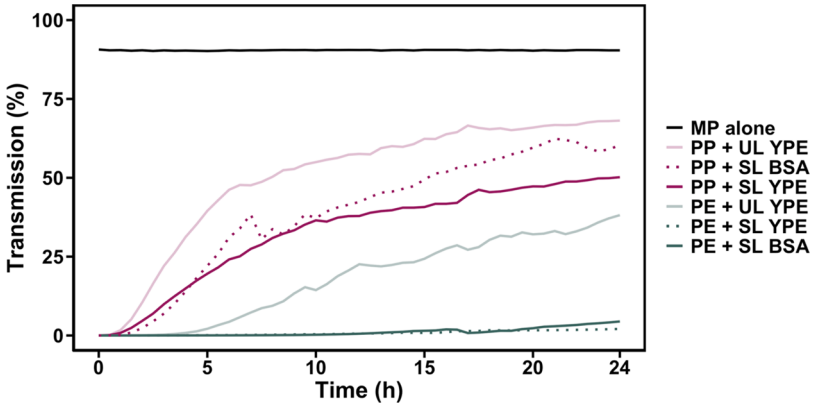

Figure 2. Creaming kinetics of PE and PP microplastics with and without proteins measured by turbidimetry. The light transmission was averaged from a 5 to 18 mm sample height and is represented as a function of time (one measurement every 30 min during 24 h). The stabilization effects of unsaturated layers (UL) and saturated layers (SL) of YPE (line) and BSA (dots) proteins are compared.

https://doi.org/10.1021/acs.langmuir.2c03237
Langmuir XXXX, XXX, XXX−XXX

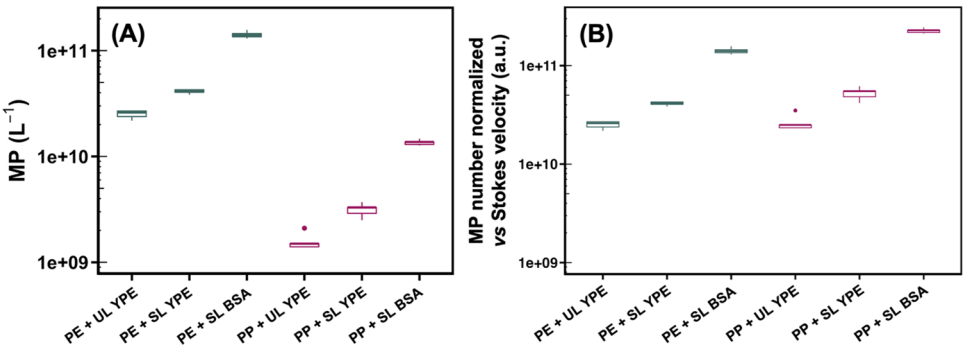

Figure 3. (A) Number of stable PE and PP microplastics per liter in phosphate buffer 100 mM, pH 7.0 after 24 h of creaming. (B) Same data after normalization by theoretical Stokes velocities (see Table S5).

eventual stabilization phase. The corresponding characteristic times were determined (Table S4). The lag phase is the time during which the transmission is stable, before a strong transmission evolution due to the creaming process itself. The lag phase also corresponds to a decrease of backscattering intensity (Supporting Information Figure S12), which can be associated with particle aggregation or clarification of the solution.[63,64] Then, if the analysis time is sufficient for the system, we can identify a stop of creaming corresponding to the stabilization phase.

For PE and PP MPs without proteins, transmission is maximum from the start of the analysis (90%), which indicates that there are no MPs in solution. With proteins on the contrary, transmission is null at time 0, indicating that the MPs are well dispersed in solution. The kinetic evolution then depends on the samples, for which three different behaviors were observed (Figure 2):

(i) For a protein SL on PE (YPE and BSA), transmission remains close to zero during all of the experiment time, indicating that a high-weight fraction of MPs remained in the solution for at least 24 h. A clarification of the dispersion was, however, observed in backscattering, which suggests a rapid creaming of the largest objects, either remaining after mixing or formed by particle aggregation.

(ii) For a protein UL on PE, the transmission is recovered after a long lag phase, indicating the passage from a concentrated to a diluted regime.[64] The backscattering data (Supporting Figure S12) show the same behavior as SL, suggesting as well the creaming of the largest particles. The slopes of the creaming phase equation (Table S4) show that the creaming is significantly slower for protein UL on PE than for PP even with an SL.

(iii) Finally, for both SL and UL on PP, the lag phase is very short, followed by a rapid increase up to a plateau value of the transmission. In the final state, we observed the presence of a gradient of particles in backscattering, corresponding to their progressive individual migration toward the air−liquid interface. This effect was specific to PP. No gradient was visible in backscattering for PE.

These results show differences in stability: most PP particles are immediately unstable in all of the studied conditions, whereas PE particles are still stable after 24 h when covered by a protein SL. This indicates that the protein layer has a strong stabilizing effect when the layer is saturated, but is less efficient for PP particles, possibly due to their larger size and lower density (d_{PP} = 0.90 and d_{PE} = 0.97). We also observed that, after creaming of PE or PP, it is possible to disperse them again very quickly just by homogenization of the sample (data not shown).

The data obtained by turbidimetry are difficult to connect to particle numbers. To obtain quantitative information about the number of stabilized MPs after 24 h, we determined their concentration by optical microscopy using counting chambers (Figure 3A). This approach allows us to count MPs stabilized by a saturated protein layer down to a diameter of 1−2 μm. Normalizing the measured particle number with respect to their theoretical Stokes creaming velocity (see Figure 3B and Table S5) allows us to unravel the different contributions of density, size, and protein corona Three observations can be made: (i) PE particles are stabilized in higher numbers compared to PP, and this effect is mainly due to their difference in Stokes behavior; (ii) a saturated corona (SL) favors MP dispersion independently of their Stokes behavior; and (iii) despite a lower quantity of adsorbed proteins (Figure 1), the model BSA layer allows a better dispersion and stabilization of MPs.

The number of particles in Figure 3A reaches 1×10^{11} MPs per liter for PE. This is in the same range as the number of polyethylene nanoparticles released by facial scrubs[65] (3×10^{11} L^{-1}) and single-use beverage cups[66] (5×10^{11} L^{-1}) for normal use, which suggests that a CCC in this range may exist for MPs. However, in the environment, the quantity of MPs is much lower from 10^{-5} to 10^{5} L^{-1} according to the sites and method of sampling.[67−69]

***In Situ* Imaging of the Protein Corona on Microplastics.** To understand why more particles can be dispersed depending on the corona saturation and type of polymer, (Figure 3), we analyzed the microscopic properties of the protein layer that forms on dispersed PE and PP MPs in UL and SL conditions. This *in situ* analysis was done using the intrinsic fluorescence of aromatic residues in proteins by synchrotron radiation deep UV (SR-DUV) fluorescence microscopy, allowing for single particle analysis with a theoretical spatial resolution of 0.11 μm (see Materials and Methods section).

The stabilized MPs were collected in solution (without the cream) after 4 h of mixing followed by a creaming of 24 h for PE and 3 h for PP. In the case of PP, this duration corresponds to a transitory system where enough stable particles were available for analysis. For longer durations, creaming becomes predominant.

The visible and DUV fluorescence images of the YPE protein corona formed on PE and PP MPs are shown in Figure 4. In the first fluorescence image (30 s), the fluorescence

https://doi.org/10.1021/acs.langmuir.2c03237
Langmuir XXXX, XXX, XXX−XXX

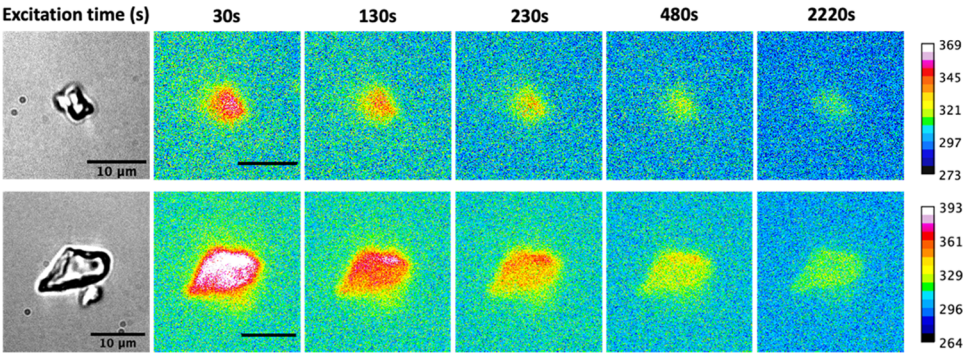

Figure 4. *In situ* SR-DUV imaging of the YPE protein corona stabilizing PE and PP microplastics in solution in SL conditions. Left: visible image of PE (top) and PP (bottom) microplastics. Left to right: DUV fluorescence images during continuous DUV illumination from 0 to 37 min ($\lambda_{excitation}$ = 265 nm, $\lambda_{emission}$ = [329-351] nm). All of the images are shown at the same scale (scale bar 10 μm).

intensity comes mainly from the adsorbed proteins following excitation at 265 nm, with limited contributions from the MPs themselves, as shown by the three-dimensional (3D) excitation−emission maps of PE, PP, and proteins measured in the same conditions (Figure S10). To confirm that the setup can map the fluorescence of the protein corona on single MPs, we performed a bleaching experiment. The evolution of the fluorescence during 37 min of continuous DUV illumination of PE and PP microplastics with a saturated YPE corona (SL) is shown in Figure 4. A clear decrease of the fluorescence intensity localized on the particles was observed due to the photobleaching of tryptophan fluorescence. Interestingly, no substitution of the bleached proteins by fluorescent-free proteins from the surrounding solution was observed in this time scale. SR-DUV imaging is thus well adapted for the *in situ* imaging of the protein corona on MPs at a micrometer scale.

Using this setup, we imaged the YPE and BSA protein corona on PE and PP MPs in solution for an acquisition time of 30 s. A minimum of 30 particles were analyzed in each condition.

Three parameters were calculated by image analysis:

- The relative protein quantity determined from the fluorescence intensity after particle delineation as a function of the protein concentration in solution. This parameter corresponds to the number of pixels for one particle multiplied by their intensity and divided by the particle surface (eq S1). It is not possible to compare the relative protein quantity on PE and PP, as we cannot exclude some fluorescence quenching by one material or another, or to compare BSA and YPE because of different intrinsic fluorescence properties.
- The particle coverage corresponds to the area covered by proteins (excluding free proteins in solution) divided by the particle surface (eq S2). A sufficient quantity of adsorbed proteins is necessary to obtain a good signal-to-noise ratio allowing precise thresholding.
- The corona heterogeneity corresponds to the standard deviation of the pixel fluorescence intensity of adsorbed proteins (eq S3).

The relative protein quantity is shown in Figure S13 for YPE-SL and -UL conditions. For both MPs we observe a higher relative protein quantity in saturation conditions (p-values = 6.2×10^{-3} for PE and 7.8×10^{-3} for PP). This result shows that, on average, the macroscopic behavior observed with the adsorption isotherms is coherent with observations at the microscopic scale, even though the amount of adsorbed proteins can vary from the least covered particles to more covered ones by 10 times. Such a wide distribution of intensities is not unknown.[70]

The protein coverage rate of YPE and BSA on PE and PP MPs is shown in Figure 5A. The median coverage rate is >1 in almost all conditions. We observe a distinct behavior for one condition only: YPE unsaturated corona on PE. In that case, the coverage rate is <1 and significantly lower than for the YPE saturated condition (p-value = 1.1×10^{-2}) with a value below

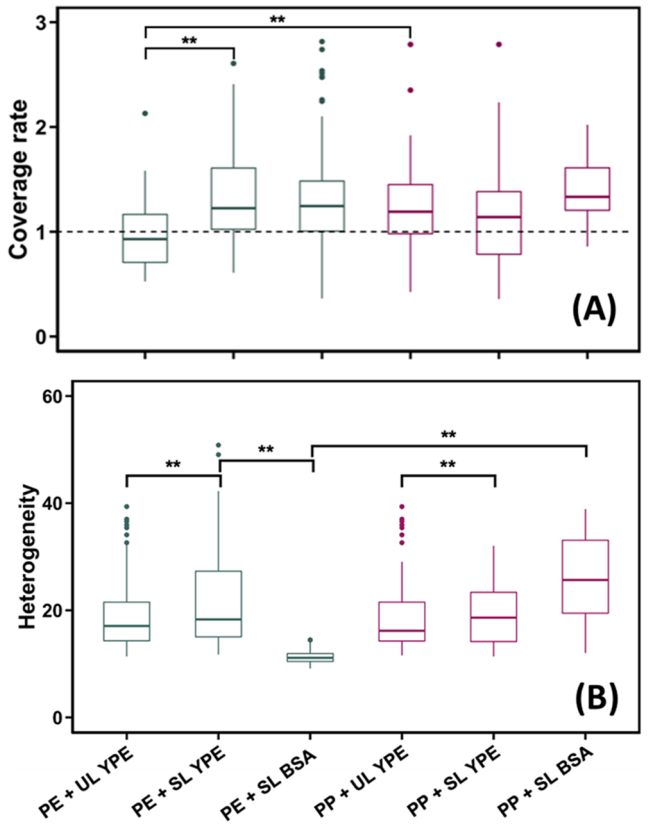

Figure 5. Protein corona properties on PE and PP microplastics in SL and UL conditions measured by SR-DUV imaging of single particles. (A) Protein coverage rate of YPE and BSA. Number of analyzed particles from left to right: 39, 53, 131, 58, 32, and 42 (**p < 0.05). (B) Heterogeneity measured as the intensity standard deviation of adsorbed YPE and BSA fluorescence. Number of analyzed particles from left to right: 40, 53, 133, 61, 32, and 42 (**p < 0.05).

https://doi.org/10.1021/acs.langmuir.2c03237
Langmuir XXXX, XXX, XXX−XXX

1 (signature of a partial layer). This result suggests that a partial protein coverage, which is an unsaturated protein layer with partially uncovered plastic surfaces, was observed at a microscopic scale for PE but not for PP in macroscopically unsaturated conditions. This result suggests also, on average, that either adsorption is less efficient on the PE surface than on the purely hydrophobic PP surface, or that PP particles that are not fully covered by proteins are not stable enough and are trapped in the cream instead. Even if these hypotheses must be tempered because of the variability observed between particles, they highlight possible differences between macroscopic observations and the heterogeneity observed at the micrometer and single-particle scale.

This result shows that this imaging method is capable of identifying changes in the corona structure. It also shows, by comparison with Figure 3, that a complete corona is not mandatory for the stabilization of PE MPs.

The corona heterogeneity, calculated as the standard deviation of the fluorescence intensity of adsorbed proteins, is shown in Figure 5B. PE and PP samples with a BSA corona show the most striking differences, with PE particles exhibiting a lower corona heterogeneity compared to PP. Combined with the indication of m_∞, this suggests a completely different organization in the BSA corona on PE and PP. It is tempting to connect the high degree of homogeneity (Figure 5B) and the high coverage (Figure 5A) to the fact that the PE sample with BSA also has the highest amount of stable particles after 24 h. (Figure 3)

More generally, for the same material, a higher relative protein quantity and protein coverage at the microscopic scale are related to a higher number of stabilized and dispersed MPs (Figure 3). The comparison between the total amount of adsorbed proteins on PE and PP (by macroscopic measurements) also shows that the absolute amount of adsorbed proteins is not a predictor of the stabilizing effect, as PP adsorbs more proteins per unit area but is less stable than PE MPs. Alternatively, the corona structure may play a key role in MP stabilization, thus requiring other approaches to analyze the protein corona at a microscopic scale.

The direct imaging (*i.e.*, without labeling) of adsorbed proteins by SR-DUV fluorescence provides an interesting insight into the study of the protein corona structure. Indeed, previous *in situ* corona studies relied either on complex microscopic strategies or on radiation diffusion technics.[71−73] Such techniques are appropriate for thickness measurements, but they rarely give access to inter- and intraparticle corona heterogeneities, a parameter that may be crucial to understand the biological response.[74]

Why Do Some Microplastics Cream Faster than Others? In the studied samples, some particles were stable in solution for several days, while others were quickly destabilized and creamed. Our observations suggest that the most stable MPs are always isolated particles, as no aggregates were visible in the suspension by optical microscopy (for hundreds of observed particles). By contrast, we observed a mixture of aggregates (Figure 8, discussed later) and isolated particles in the cream. Here, we investigated whether the corona properties were different between these two families of isolated particles (dispersed *versus* creamed). The saturated condition (SL) was chosen to carry out this study.

The protein coverage rate measured for dispersed or creamed PE and PP MPs is shown in Figure 6A. The coverage rate is significantly different between the dispersed and the

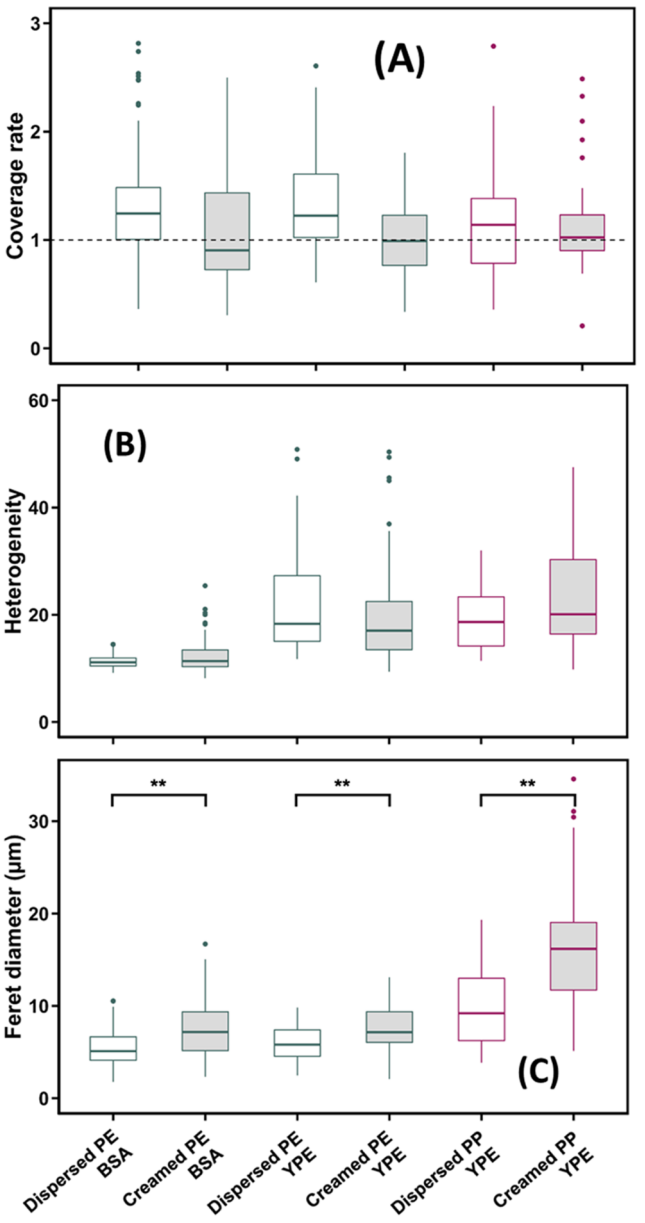

Figure 6. Comparison between dispersed microplastics (in the infranatant, white box) and creamed PE and PP microplastics (gray box) by SR-DUV imaging of single particles. Number of analyzed particles from left to right: 133, 36, 53, 67, 32, and 55. (**p-value < 0.05). (A) Protein coverage rate. (B) Protein corona heterogeneity. (C) Feret diameters.

creamed PE particles with YPE: the median is, respectively, 1.25 and 1.0 with a p-value = 1.7×10^{-2}, corresponding to a thicker protein layer on the dispersed PE compared to the creamed PE. By contrast, for PP with YPE or BSA, and for PE with BSA, the coverage rate, around 1, is not significantly different for the two populations. Therefore, this parameter is not the main determinant for MP creaming/dispersion.

The corresponding corona heterogeneity is shown in Figure 6B. No significant difference is observed between the dispersed and the creamed particles for one type of protein for this indicator.

Then, we measured the MP size in the dispersed phase and in the creamed phase (Figure 6C). It appears that the particles are systematically smaller in the infranatant than in the cream

https://doi.org/10.1021/acs.langmuir.2c03237
Langmuir XXXX, XXX, XXX−XXX

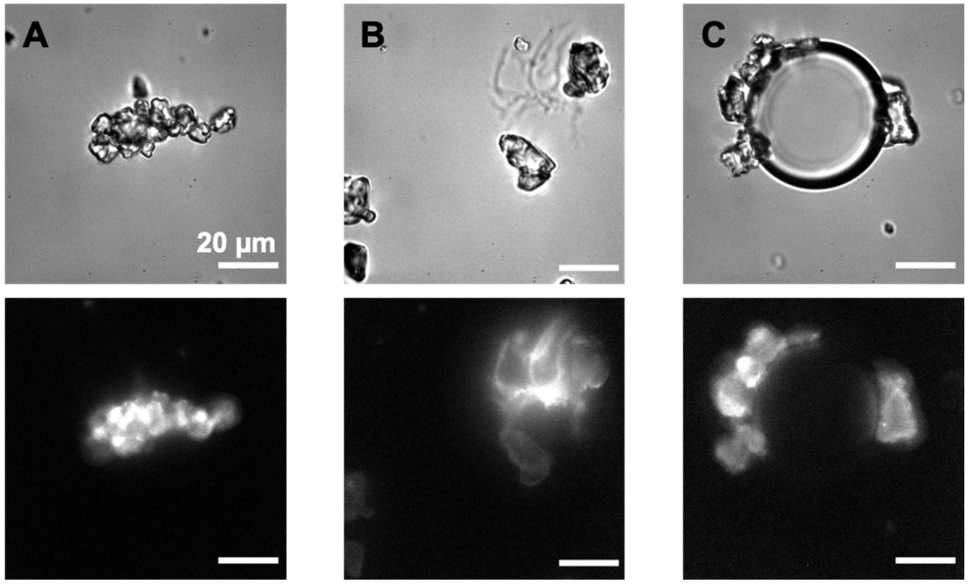

Figure 7. Bright-field (top) and DUV fluorescence (bottom) images of microplastic assemblies observed after PP creaming in YPE solution: aggregates of MPs with their protein corona (A), bridging of MPs by protein aggregation, without direct MP−MP contact (B), and air bubbles surrounded by MPs (C). All of the observations were done with YPE.

with a p-value of 1.3×10^{-6}, 4.7×10^{-5}, and 2.0×10^{-6}, respectively, for BSA on PE, YPE on PE, and YPE on PP. Moreover, PP MPs, which exhibit lower stability in aqueous solutions, are both larger and less dense than PE. Therefore, smaller and denser MPs are more stable in solution, which is in accordance with the Stokes law.[75]

These results demonstrate that protein adsorption is necessary for the dispersion of microplastics and their stabilization, but that particle size and density are nonetheless important parameters favoring their destabilization and creaming.

In addition to isolated particles, microscopic observations of the creamed MPs revealed for YPE three complex assemblies: MP aggregates, MP bridging by protein aggregation without direct MP−MP contact, and air bubbles surrounded by MPs (Figure 7). If these MP assemblies form in the solution, they can increase the kinetics of creaming because of the increase in the object size (aggregation, bridging) or the decrease in the object density (air bubbles). Alternatively, if they form after creaming, they can stabilize the creamed MPs, making it even more difficult to resuspend them, unless the biological component is degraded by other mechanisms.

All of these complexes include proteins, as shown by the fluorescence image of tryptophan and tyrosine residues. The stabilization of bubbles by MPs in the cream is driven by the protein corona since it is not observed in the absence of proteins or MPs in solution. Like a Pickering emulsion where liquid drops are stabilized by insoluble particles at their interface in another liquid phase, here, a gas bubble is stabilized over long periods by protein-covered plastic particles. In aquatic environments, scum is formed because of waves that introduce air in the superficial water layer where bubbles can be further stabilized by biomolecules, potentially forming the same type of assemblies. Therefore, it is likely that MPs in environmental waters, stabilized by a protein corona or ecocorona, also stabilize air bubbles formed by flows. Such microbubbles then become highly susceptible to aerosolization of MPs from the water to the air compartment. This transfer mechanism could contribute in part to the presence of MPs in the atmosphere.[76]

Can We Use the Corona to Remove Microplastics from a Solution? Removing plastics from drinking water is becoming necessary due to the amount of microplastics detected and their potential health effects.[77] Presently, most strategies focus on filtration. Because of the sensitivity of the MP colloidal stability with respect to the protein corona shown in this work, we consider that one strategy to abate microplastics may be altering the protein corona to induce MP creaming (for MPs with densities <1) or sedimentation (for MPs with densities >1) and their subsequent removal from water. This strategy is similar to the ones used in wine fining: proteins are artificially introduced in the solution to trap tannins by coprecipitation.[78]

To test this strategy with PE MPs, we selected two methods that are known to promote protein destabilization: (i) precipitation induced by high salt contents, (ii) thermal denaturation, leading to protein aggregation. We used ammonium sulfate at two concentrations on one hand, and heating for 1 h at 80 °C on the other hand. Ammonium sulfate was chosen because it is known to induce protein precipitation through electrostatic screening without denaturation. MPs were dispersed (4 h of mixing) in solution prior to treatments in the conditions YPE-SL. We analyzed the quantity of stable MPs after the destabilization treatment followed by 24 h of creaming using the counting chambers (Figure 8). For 14% w/v of ammonium sulfate (equals to 25% salt saturation,[45] 1.1 M), we only observed a slight decrease in the number of stable MPs (4×10^{10} for the reference and 3×10^{10} particles/L after ammonium sulfate addition). With 70% $(NH_4)_2SO_4$ (100% saturation, 5.3 M), MPs are strongly destabilized, resulting in the creaming of about 95% of MPs after 24 h. A similar effect was observed following the thermal treatment at 80 °C for 1 h.

Salting out and thermal treatments quickly destabilize the MP dispersion.

For the salting out, the fact that 1.1 M ammonium sulfate has no effect suggests that it does not act solely by electrostatic

https://doi.org/10.1021/acs.langmuir.2c03237
Langmuir XXXX, XXX, XXX−XXX

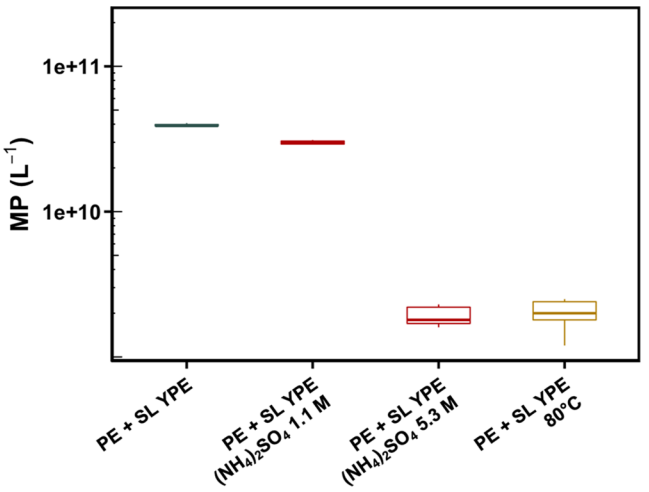

Figure 8. Number of stable PE microplastics after the destabilizing treatment by high ammonium salt concentration or high temperature followed by 24 h of creaming.

screening but also likely by enhancing the hydrophobic effect.[79,80] For the thermal treatment, destabilization is probably caused by protein denaturation and bridging between particles, favoring creaming.

These destabilization tests show that, by controlling the protein corona, it becomes possible to accelerate PE MP creaming to collect and eliminate them more easily than with innovative though complex filtration schemes.[81] Indeed, the combination of corona formation with the thermal treatment presented here may be very simple to implement for drinking water where industrial solutions of depollution are not available.

Would the same strategy work for nanoplastics? One can assume that the largest surface area of nanoplastics would also favor the adsorption of proteins, and hence the possibility to control their stability in solution by direct action on the protein corona.

What are the Underlying Dispersion/Stabilization Mechanisms? Studies on purified proteins have shown the role of the protein corona on nanoparticle stability in solution.[11,24,32,82,83] Depending on the protein charge and the salt concentration in the medium, it is possible to induce nanoparticle aggregation or, on the contrary, stabilization in solution. It has also been shown that a complete corona, at the macroscopic scale, is required to ensure steric stabilization.[82] However, information at the microscopic scale of particles is scarce.

In the case of MPs mixed with a protein extract composed of thousands of different proteins, we observed that protein adsorption favors the dispersion and the stabilization of hydrophobic MPs in aqueous media.

We tried to explain these observations using the four main phenomena described below.

Surface Tension. The studied MPs are particularly hydrophobic. In water, they stay at the air/water interface to minimize interfacial free energy.[84] Another way to minimize the interfacial energy is the interaction with surfactants: amphiphilic molecules surround the MPs, creating a bridge between hydrophobic particles and water. Adsorbed proteins act as a biological surfactant (Table S3) that makes the polymer surface more hydrophilic. In the case studied here, the lowest surface tension provided by adsorbed proteins allows for MP penetration in aqueous solutions, once they are covered with their partial or full protein layer.[85]

Physical Properties of Particles. Size and density remain the most important properties to predict MP behavior once they have entered the water. Indeed, PP particles, that are larger and less dense, disperse systematically to a lower concentration and cream faster (Figure 3A, Table S4). However, the protein corona can modulate this Stokes behavior (Figure 3B). Indeed, the migration speed measured by Turbiscan is, in most cases, significantly lower than the one predicted by the Stokes law alone (even taking into account the corona thickness, see Table S5) and depends on the corona quality. As a result, PP particles, when covered by a high-quality corona in terms of thickness and homogeneity, such as a BSA corona, can disperse in a comparable concentration as PE covered by a low-quality one.

Electrostatic Repulsion. Colloidal stabilization phenomena are usually explained by the DLVO theory.[12,13] Even though the studied MPs are uncharged polyolefins, when proteins adsorb on their surface, the objects become charged. These charges create a DLVO potential barrier, which ensures electrostatic repulsions that may prevent MP aggregation.

We indeed observed a slight decrease in particle stability with 1.1 M ammonium sulfate (Figure 8), but this effect is small compared to the generally observed CCC (in the range of a few tens or hundreds mM, depending on the ion valence and the particle properties).[82,86,87]

Furthermore, ζ potential measurements on PE (such measurements were not possible on PP owing to their faster creaming) show that partial and complete YPE layers have the same potential even though they do not present the same stabilization and that this potential is too low (−10 mV) to provide an efficient stabilization by itself.

Another observation suggesting that DLVO is not sufficient to explain the stability is the creaming reversibility. Indeed, for destabilization caused by a lack of electrostatic repulsions, particles are irreversibly aggregated. In our case, the creaming is reversible and particles are quickly redispersed by gentle homogenization.

These three elements suggest the existence of an additional stabilizing mechanism.

Steric Hindrance. Steric hindrance may provide the key stabilization mechanism. A recent publication suggests a similar effect for polymer brushes and protein corona, ensuring a steric repulsion of the particles.[14] Proteins are also polymers and can generate a steric hindrance if they are adsorbed on particles.[83,88]

Steric hindrance can explain why the corona presenting the highest coverage rate (Figure 6A) is also associated with MPs that will be dispersed at the highest concentration. Steric hindrance will also be less efficient if the corona is not complete (allowing bridging between particles).[89]

We also introduced in this work some notions about the corona quality. It encompasses the traditional notion of saturation that comes from isotherm measurements but is not limited to it. Here, we add the notions of coverage rate and homogeneity, two parameters that require a microscopic description of the corona and single particle analysis. In this respect, purified proteins, like BSA seem to produce a corona of higher quality than complex protein extracts.

In the context of colloidal stabilization, the quality of the corona allows uniform charge repartition as well as an important density of the polymer chain, ensuring electrostatic

https://doi.org/10.1021/acs.langmuir.2c03237
Langmuir XXXX, XXX, XXX−XXX

and steric repulsions, respectively. However, the importance of the corona quality probably extends beyond this context, and it may also be a determinant in its own stability and in the biological response it can trigger.

CONCLUSIONS

In this study, we showed that the protein corona enables the dispersion of an important quantity of low density and highly hydrophobic MPs. Proteins act as surfactants that make the surface more hydrophilic and deagglomerate microplastics, allowing them to acquire a colloidal behavior as stabilized single particles. By generating sufficient repulsions, the protein corona allows hydrophobic MPs to remain dispersed in the aqueous suspension during long periods. Moreover, the stabilization increases with the quality of the protein corona, a parameter we could define at a microscopic scale by *in situ* label-free imaging of the protein corona on single particles in solution.

The microplastic stability is complex and depends on different mechanisms among which are the wettability, the particle intrinsic properties, and the steric hindrance. By controlling these parameters and the properties of the protein corona, it becomes possible to manipulate microplastics in and out solutions, a strategy that can be investigated for the removal of the MP pollution.

ASSOCIATED CONTENT

Supporting Information

The Supporting Information is available free of charge at https://pubs.acs.org/doi/10.1021/acs.langmuir.2c03237.

> Characterization of PE and PP microplastics (microscopic images, Feret diameter distribution, FTIR spectra, XPS spectra, mapping by confocal Raman microscopy, SAXS profiles, 3D fluorescence excitation−emission maps); photographs of dispersion; quantitative data determined from the turbidimetry profiles; image treatment; equations used to determine the corona properties; and additional tables (PDF)

AUTHOR INFORMATION

Corresponding Authors

Marion Schvartz − *Université Paris-Saclay, CEA, CNRS, NIMBE, F-91191 Gif Sur Yvette, France; Institut des Molécules et Matériaux du Mans (IMMM), UMR 6283 CNRS, Le Mans Université, 72085 Le Mans, France*; Email: marion.schvartz@cea.fr

Jean-Philippe Renault − *Université Paris-Saclay, CEA, CNRS, NIMBE, F-91191 Gif Sur Yvette, France*; orcid.org/0000-0003-2555-5857; Email: jean-philippe.renault@cea.fr

Authors

Florent Saudrais − *Université Paris-Saclay, CEA, CNRS, NIMBE, F-91191 Gif Sur Yvette, France*

Stéphanie Devineau − *Université Paris Cité, CNRS, Unité de Biologie Fonctionnelle et Adaptative, F-75013 Paris, France*; orcid.org/0000-0002-1133-5223

Stéphane Chédin − *Université Paris-Saclay, CEA, CNRS, NIMBE, F-91191 Gif Sur Yvette, France; Université Paris-Saclay, CEA, CNRS, Institute for Integrative Biology of the Cell (I2BC), 91198 Gif-sur-Yvette, France*

Frédéric Jamme − *Synchrotron SOLEIL, 91190 Gif sur Yvette, France*; orcid.org/0000-0002-7398-7868

Jocelyne Leroy − *Université Paris-Saclay, CEA, CNRS, NIMBE, F-91191 Gif Sur Yvette, France*

Karol Rakotozandriny − *Université Paris-Saclay, CEA, CNRS, Institute for Integrative Biology of the Cell (I2BC), 91198 Gif-sur-Yvette, France*

Olivier Taché − *Université Paris-Saclay, CEA, CNRS, NIMBE, F-91191 Gif Sur Yvette, France*

Guillaume Brotons − *Institut des Molécules et Matériaux du Mans (IMMM), UMR 6283 CNRS, Le Mans Université, 72085 Le Mans, France*; orcid.org/0000-0003-3832-3932

Serge Pin − *Université Paris-Saclay, CEA, CNRS, NIMBE, F-91191 Gif Sur Yvette, France*

Yves Boulard − *Université Paris-Saclay, CEA, CNRS, Institute for Integrative Biology of the Cell (I2BC), 91198 Gif-sur-Yvette, France*

Complete contact information is available at: https://pubs.acs.org/10.1021/acs.langmuir.2c03237

Notes

The authors declare no competing financial interest.

ACKNOWLEDGMENTS

The polyethylene and polypropylene microplastics were provided by Clariant. Fluorescence imaging using synchrotron radiation was carried out, thanks to SOLEIL (DISCO beamline, proposal number 20210214). The authors acknowledge the Raman—AFM Platform (MPQ, Université Paris Cité) funded by ANR-18-IDEX-0001, IdEx Université Paris Cité. K.R. was funded by the PTC−ID from CEA. The authors acknowledge the LEDNA laboratory (NIMBE, CEA) for the use of their Turbiscan analyzer. This project has received funding from The French National Research Program for Environmental and Occupational Health of Anses (2018/1/194) from the European Union's Horizon 2020 Research and Innovation Programme under the grant agreement No. 965367 (Plastics Fate) and from the MITI of CNRS (CSP). This work was supported by a Ph.D. grant overseen by the CEA and the Région Pays de la Loire.

REFERENCES

(1) Gewert, B.; Plassmann, M. M.; MacLeod, M. Pathways for degradation of plastic polymers floating in the marine environment. *Environ. Sci. Process. Impacts* **2015**, *17*, 1513−1521.

(2) Garvey, C. J.; Impéror-Clerc, M.; Rouzière, S.; et al. Molecular-Scale Understanding of the Embrittlement in Polyethylene Ocean Debris. *Environ. Sci. Technol.* **2020**, *54*, 11173−11181.

(3) Meides, N.; Menzel, T.; Poetzschner, B.; et al. Reconstructing the Environmental Degradation of Polystyrene by Accelerated Weathering. *Environ. Sci. Technol.* **2021**, *55*, 7930−7938.

(4) Julienne, F. Fragmentation des plastiques: effet de l'environnement et de la nature du polymère sur la taille et la forme des fragments générés. Thesis, Le Mans Université, 2019.

(5) Andrady, A. L. Microplastics in the marine environment. *Mar. Pollut. Bull.* **2011**, *62*, 1596−1605.

(6) Galloway, T. S.; Cole, M.; Lewis, C.; et al. Interactions of microplastic debris throughout the marine ecosystem. *Nat. Ecol. Evol.* **2017**, *1*, No. 0116.

(7) Gigault, J.; Halle, A. t.; Baudrimont, M.; et al. Current opinion: What is a nanoplastic? *Environ. Pollut.* **2018**, *235*, 1030−1034.

(8) Chae, Y.; An, Y.-J. Effects of micro- and nanoplastics on aquatic ecosystems: Current research trends and perspectives. *Mar. Pollut. Bull.* **2017**, *124*, 624−632.
(9) Isobe, A.; Azuma, T.; Cordova, M. R.; et al. A multilevel dataset of microplastic abundance in the world's upper ocean and the Laurentian Great Lakes. *Microplast. Nanoplast.* **2021**, *1*, No. 16.
(10) Khatmullina, L.; Chubarenko, I. Transport of marine microplastic particles: why is it so difficult to predict? *Anthr. Coasts* **2019**, *2*, 293−305.
(11) Dong, Z.; Hou, Y.; Han, W.; et al. Protein corona-mediated transport of nanoplastics in seawater-saturated porous media. *Water Res.* **2020**, *182*, No. 115978.
(12) Derjaguin, B.; Landau, L. Theory of the stability of strongly charged lyophobic sols and of the adhesion of strongly charged particles in solutions of electrolytes. *Prog. Surf. Sci.* **1993**, *43*, 30−59.
(13) Verwey, E.; Overbeek, T. *Theory of the Stability of Lyophobic Colloids: The Interaction of Sol Particles Having an Electric Double Layer*, 1948.
(14) Witzmann, T.; Ramsperger, A. F. R. M.; Wieland, S.; et al. Repulsive interactions of eco-corona-covered microplastic particles quantitatively follow modeling of polymer brushes. *Langmuir* **2022**, *38*, 8748−8756.
(15) Venel, Z.; Tabuteau, H.; Pradel, A.; et al. Environmental Fate Modeling of Nanoplastics in a Salinity Gradient Using a Lab-on-a-Chip: Where Does the Nanoscale Fraction of Plastic Debris Accumulate? *Environ. Sci. Technol.* **2021**, *55*, 3001−3008.
(16) Grolimund, D.; Elimelech, M.; Borkovec, M. Aggregation and deposition kinetics of mobile colloidal particles in natural porous media. *Colloids Surf., A* **2001**, *191*, 179−188.
(17) Cao, J.; Yang, Q.; Jiang, J.; et al. Coronas of micro/nano plastics: a key determinant in their risk assessments. *Part. Fibre Toxicol.* **2022**, *19*, No. 55.
(18) Kooi, M.; Nes, E. H.; van Scheffer, M.; Koelmans, A. A. Ups and Downs in the Ocean: Effects of Biofouling on Vertical Transport of Microplastics. *Environ. Sci. Technol.* **2017**, *51*, 7963−7971.
(19) Kaiser, D.; Kowalski, N.; Waniek, J. J. Effects of biofouling on the sinking behavior of microplastics. *Environ. Res. Lett.* **2017**, *12*, No. 124003.
(20) Gunsolus, I. L.; Haynes, C. L. Analytical Aspects of Nanotoxicology. *Anal. Chem.* **2016**, *88*, 451−479.
(21) Abarca-Cabrera, L.; Fraga-García, P.; Berensmeier, S. Bio-nano interactions: binding proteins, polysaccharides, lipids and nucleic acids onto magnetic nanoparticles. *Biomater. Res.* **2021**, *25*, No. 12.
(22) Ke, P. C.; Lin, S.; Parak, W. J.; Davis, T. P.; Caruso, F. A Decade of the Protein Corona. *ACS Nano* **2017**, *11*, 11773−11776.
(23) Gopinath, P. M.; Saranya, V.; Vijayakumar, S.; et al. Assessment on interactive prospectives of nanoplastics with plasma proteins and the toxicological impacts of virgin, coronated and environmentally released-nanoplastics. *Sci. Rep.* **2019**, *9*, No. 8860.
(24) Gebauer, J. S.; Malissek, M.; Simon, S.; et al. Impact of the Nanoparticle−Protein Corona on Colloidal Stability and Protein Structure. *Langmuir* **2012**, *28*, 9673−9679.
(25) Wheeler, K. E.; Chetwynd, A. J.; Fahy, K. M.; et al. Environmental dimensions of the protein corona. *Nat. Nanotechnol.* **2021**, *16*, 617−629.
(26) Xu, L.; Xu, M.; Wang, R.; et al. The Crucial Role of Environmental Coronas in Determining the Biological Effects of Engineered Nanomaterials. *Small* **2020**, *16*, No. 2003691.
(27) Akhter, M. H.; Khalilullah, H.; Gupta, M.; et al. Impact of Protein Corona on the Biological Identity of Nanomedicine: Understanding the Fate of Nanomaterials in the Biological Milieu. *Biomedicines* **2021**, *9*, 1496.
(28) Marichal, L.; Degrouard, J.; Gatin, A.; et al. From Protein Corona to Colloidal Self-Assembly: The Importance of Protein Size in Protein−Nanoparticle Interactions. *Langmuir* **2020**, *36*, 8218−8230.
(29) Bharti, B.; Meissner, J.; Klapp, S. H. L.; Findenegg, G. H. Bridging interactions of proteins with silica nanoparticles: The influence of pH, ionic strength and protein concentration. *Soft Matter* **2014**, *10*, 718−728.
(30) Moerz, S. T.; Kraegeloh, A.; Chanana, M.; Kraus, T. Formation Mechanism for Stable Hybrid Clusters of Proteins and Nanoparticles. *ACS Nano* **2015**, *9*, 6696−6705.
(31) Li, X.; He, E.; Jiang, K.; Peijnenburg, W. J. G. M.; Qiu, H. The crucial role of a protein corona in determining the aggregation kinetics and colloidal stability of polystyrene nanoplastics. *Water Res.* **2021**, *190*, No. 116742.
(32) Li, X.; He, E.; Xia, B.; et al. Protein corona-induced aggregation of differently sized nanoplastics: impacts of protein type and concentration. *Environ. Sci. Nano* **2021**, *8*, 1560−1570.
(33) Michels, J.; Stippkugel, A.; Lenz, M.; Wirtz, K.; Engel, A. Rapid aggregation of biofilm-covered microplastics with marine biogenic particles. *Proc. R. Soc. B* **2018**, *285*, 1203.
(34) Tallec, K.; Blard, O.; González-Fernández, C.; et al. Surface functionalization determines behavior of nanoplastic solutions in model aquatic environments. *Chemosphere* **2019**, *225*, 639−646.
(35) Goffeau, A.; Barrell, B. G.; Bussey, H.; et al. Life with 6000 Genes. *Science* **1996**, *274*, 546−567.
(36) Schulze, W. X. Protein analysis in dissolved organic matter: What proteins from organic debris, soil leachate and surface water can tell us - a perspective. *Biogeosciences* **2005**, *2*, 75−86.
(37) Jung-Hyun; Jeong-Yeol, Y. Protein adsorption on polymer particles. *Encycl. Surf. Colloid Sci.* **2002**, 4373−4381.
(38) Schindelin, J.; Arganda-Carreras, I.; Frise, E.; et al. Fiji: an open-source platform for biological-image analysis. *Nat. Methods* **2012**, *9*, 676−682.
(39) Mathé, C.; Devineau, S.; Aude, J. C.; et al. Structural Determinants for Protein adsorption/non-adsorption to Silica Surface. *PLoS One* **2013**, *8*, No. e81346.
(40) Klein, G.; Mathé, C.; Biola-Clier, M.; et al. RNA-binding proteins are a major target of silica nanoparticles in cell extracts. *Nanotoxicology* **2016**, *10*, 1555−1564.
(41) Bradford, M. M. A Rapid and Sensitive Method for the Quantitation of Microgram Quantities of Protein Utilizing the Principle of Protein-Dye Binding. *Anal. Biochem.* **1976**, *72*, 248−254.
(42) Everett, D. H. Why are Colloidal Dispersions Stable? I Basic Principles. In *Basic Principles of Colloid Science*; Royal Society of Chemistry, 1988; Chapter 2, pp 16−29.
(43) Jamme, F.; Villette, S.; Giuliani, A.; et al. Synchrotron UV Fluorescence Microscopy Uncovers New Probes in Cells and Tissues. *Microsc. Microanal.* **2010**, *16*, 507−514.
(44) Giuliani, A.; Jamme, F.; Rouam, V.; et al. DISCO: a low-energy multipurpose beamline at synchrotron SOLEIL. *J. Synchrotron Radiat.* **2009**, *16*, 835−841.
(45) Duong-Ly, K. C.; Gabelli, S. B. Salting out of Proteins Using Ammonium Sulfate Precipitation. In *Methods in Enzymology*; Elsevier, 2014; Vol. *541*, pp 85−94.
(46) Bernal, V.; Jelen, P. Thermal Stability of Whey Proteins − A Calorimetric Study. *J. Dairy Sci.* **1985**, *68*, 2847−2852.
(47) Araujo, C. F.; Nolasco, M. M.; Ribeiro, A. M. P.; Ribeiro-Claro, P. J. A. Identification of microplastics using Raman spectroscopy: Latest developments and future prospects. *Water Res.* **2018**, *142*, 426−440.
(48) Fontana, L.; Santoro, M.; Bini, R.; Vinh, D. Q.; Scandolo, S. High-pressure vibrational properties of polyethylene. *J. Chem. Phys.* **2010**, *133*, No. 204502.
(49) Karacan, İ.; Benli, H. The use of infrared-spectroscopy for the structural characterization of isotactic polypropylene fibres. *Text. Apparel* **2011**, 116−123.
(50) Gopanna, A.; Mandapati, R. N.; Thomas, S. P.; Rajan, K.; Chavali, M. Fourier transform infrared spectroscopy (FTIR), Raman spectroscopy and wide-angle X-ray scattering (WAXS) of polypropylene (PP)/cyclic olefin copolymer (COC) blends for qualitative and quantitative analysis. *Polym. Bull.* **2019**, *76*, 4259−4274.
(51) Hiejima, Y.; Kida, T.; Takeda, K.; Igarashi, T.; Nitta, K. Microscopic structural changes during photodegradation of low-density polyethylene detected by Raman spectroscopy. *Polym. Degrad. Stab.* **2018**, *150*, 67−72.

https://doi.org/10.1021/acs.langmuir.2c03237
Langmuir XXXX, XXX, XXX−XXX

(52) Jin, Y.; Kotula, A. P.; Snyder, C. R.; et al. Raman Identification of Multiple Melting Peaks of Polyethylene. *Macromolecules* **2017**, *50*, 6174−6183.
(53) Zemb, T.; Lindner, P. *Neutron, X-rays and Light. Scattering Methods Applied to Soft Condensed Matter*; Elsevier Science, 2002.
(54) Guinier, A. Direct analysis of diffraction by matter by R. Hosemann and S. N. Bagchi. *Acta Cryst.* **1964**, *86*, 463−464.
(55) Fatnassi, M.; Ben Cheikh Larbi, F.; Halary, J. L. Quantitative Analysis of Semicrystalline Blends SAXS Data: Theoretical Modeling versus Linear Correlation Function. *Int. J. Polym. Sci.* **2010**, *2010*, 1−6.
(56) Koga, M.; Watanabe, R.; Hagihara, H.; et al. Accelerated aging-induced variation of polypropylene (PP) structure studied by two-dimensional (2D) small-angle X-ray scattering (SAXS) correlation spectroscopy. *J. Mol. Struct.* **2020**, *1207*, No. 127764.
(57) Yui, N.; Suzuki, Y.; Mori, H.; Terano, M. Surface Properties of Polypropylene Films as Biomaterials. *Polym. J.* **1995**, *27*, 614−622.
(58) Marichal, L.; Klein, G.; Armengaud, J.; et al. Protein Corona Composition of Silica Nanoparticles in Complex Media: Nanoparticle Size does not Matter. *Nanomaterials* **2020**, *10*, 240.
(59) Vertegel, A. A.; Siegel, R. W.; Dordick, J. S. Silica Nanoparticle Size Influences the Structure and Enzymatic Activity of Adsorbed Lysozyme. *Langmuir* **2004**, *20*, 6800−6807.
(60) Lundqvist, M.; Sethson, I.; Jonsson, B.-H. Protein Adsorption onto Silica Nanoparticles: Conformational Changes Depend on the Particles' Curvature and the Protein Stability. *Langmuir* **2004**, *20*, 10639−10647.
(61) Young, B. R.; Pitt, W. G.; Cooper, S. L. Protein adsorption on polymeric biomaterials I. Adsorption isotherms. *J. Colloid Interface Sci.* **1988**, *124*, 28−43.
(62) Horbett, T. A.; Weathersbp, P. K.; Boffman, A. S. Hemoglobin adsorption to three polymer surfaces. *Thromb. Res.* **1978**, *12*, 319−329.
(63) Bongono, J. Caractérisation des suspensions par des méthodes optiques. In *Modélisation par réseaux de neurones*; École Nationale Supérieure des Mines de Saint-Étienne, 2010.
(64) Mengual, O. TURBISCAN MA 2000: multiple light scattering measurement for concentrated emulsion and suspension instability analysis. *Talanta* **1999**, *50*, 445−456.
(65) Enfrin, M.; Lee, J.; Gibert, Y.; et al. Release of hazardous nanoplastic contaminants due to microplastics fragmentation under shear stress forces. *J. Hazard. Mater.* **2020**, *384*, No. 121393.
(66) Zangmeister, C. D.; Radney, J. G.; Benkstein, K. D.; Kalanyan, B. Common Single-Use Consumer Plastic Products Release Trillions of Sub-100 nm Nanoparticles per Liter into Water during Normal Use. *Environ. Sci. Technol.* **2022**, *56*, 5448−5455.
(67) Li, Y.; Li, W.; Jarvis, P.; et al. Occurrence, removal and potential threats associated with microplastics in drinking water sources. *J. Environ. Chem. Eng.* **2020**, *8*, No. 104527.
(68) Wang, Z.; Lin, T.; Chen, W. Occurrence and removal of microplastics in an advanced drinking water treatment plant (ADWTP). *Sci. Total Environ.* **2020**, *700*, No. 134520.
(69) Koelmans, A. A.; Mohamed Nor, N. H.; Hermsen, E.; et al. Microplastics in freshwaters and drinking water: Critical review and assessment of data quality. *Water Res.* **2019**, *155*, 410−422.
(70) Wang, Y.; Soto Rodriguez, P. E. D.; Woythe, L.; et al. Multicolor Super-Resolution Microscopy of Protein Corona on Single Nanoparticles. *ACS Appl. Mater. Interfaces* **2022**, *14*, 37345−37355.
(71) Galdino, F. E.; Picco, A. S.; Capeletti, L. B.; Bettini, J.; Cardoso, M. B. Inside the Protein Corona: From Binding Parameters to Unstained Hard and Soft Coronas Visualization. *Nano Lett.* **2021**, *21*, No. 1c02416.
(72) Marichal, L.; Giraudon−Colas, G.; Cousin, F.; et al. Protein−Nanoparticle Interactions: What Are the Protein−Corona Thickness and Organization? *Langmuir* **2019**, *35*, 10831−10837.
(73) Sanchez-Guzman, D.; Giraudon−Colas, G.; Marichal, L.; et al. In Situ Analysis of Weakly Bound Proteins Reveals Molecular Basis of Soft Corona Formation. *ACS Nano* **2020**, *14*, 9073−9088.
(74) Feiner-Gracia, N.; Beck, M.; Pujals, S.; et al. Super-Resolution Microscopy Unveils Dynamic Heterogeneities in Nanoparticle Protein Corona. *Small* **2017**, *13*, No. 1701631.
(75) Fayed, M. E.; Otten, L. *Handbook of Powder Science & Technology*; Springer: US, 1997.
(76) Trainic, M.; Flores, J. M.; Pinkas, I.; et al. Airborne microplastic particles detected in the remote marine atmosphere. *Commun. Earth Environ.* **2020**, *1*, No. 64.
(77) Xu, Z.; Bai, X.; Ye, Z. Removal and generation of microplastics in wastewater treatment plants: A review. *J. Clean. Prod.* **2021**, *291*, No. 125982.
(78) Karamanidou, A.; Kallithraka, S.; Hatzidimitriou, E. Fining of red wines: effects on their analytical and sensory parameters. *OENO One* **2016**, *45*, No. 47.
(79) Arakawa, T.; Timasheff, S. N. Mechanism of protein salting in and salting out by divalent cation salts: balance between hydration and salt binding. *Biochemistry* **1984**, *23*, 5912−5923.
(80) Hyde, A. M.; Zultanski, S. L.; Waldman, J. H.; et al. General Principles and Strategies for Salting-Out Informed by the Hofmeister Series. *Org. Process Res. Dev.* **2017**, *21*, 1355−1370.
(81) Risch, P.; Adlhart, C. A Chitosan Nanofiber Sponge for Oyster-Inspired Filtration of Microplastics. *ACS Appl. Polym. Mater.* **2021**, *3*, 4685−4694.
(82) Sáringer, S.; Akula, R. A.; Szerlauth, A.; Szilagyi, I. Papain Adsorption on Latex Particles: Charging, Aggregation, and Enzymatic Activity. *J. Phys. Chem. B* **2019**, *123*, 9984−9991.
(83) Vasti, C.; Bedoya, D. A.; Rojas, R.; Giacomelli, C. E. Effect of the protein corona on the colloidal stability and reactivity of LDH-based nanocarriers. *J. Mater. Chem. B* **2016**, *4*, 2008−2016.
(84) Al Harraq, A.; Bharti, B. Microplastics through the Lens of Colloid Science. *ACS Environ. Au* **2022**, *2*, 3−10.
(85) Liu, X.; Wang, X.; Liang, Y.; Zhou, F. Floating behavior of hydrophobic glass spheres. *J. Colloid Interface Sci.* **2009**, *336*, 743−749.
(86) Ince-Coskun, A. E.; Ozdestan-Ocak, O. Effects of salt ions and heating on the behaviour of whey protein particle dispersions. *Food Hydrocoll.* **2020**, *101*, No. 105433.
(87) Cao, T.; Szilagyi, I.; Oncsik, T.; Borkovec, M.; Trefalt, G. Aggregation of Colloidal Particles in the Presence of Multivalent Co-Ions: The Inverse Schulze−Hardy Rule. *Langmuir* **2015**, *31*, 6610−6614.
(88) Likos, C. N.; Vaynberg, K. A.; Löwen, H.; Wagner, N. J. Colloidal Stabilization by Adsorbed Gelatin. *Langmuir* **2000**, *16*, 4100−4108.
(89) Gregory, J.; Barany, S. Adsorption and flocculation by polymers and polymer mixtures. *Adv. Colloid Interface Sci.* **2011**, *169*, 1−12.

https://doi.org/10.1021/acs.langmuir.2c03237
Langmuir XXXX, XXX, XXX−XXX